

## Accepted Manuscript

Title: Enhanced Electrocatalytic Performance for Methanol Oxidation with a Magnéli Phase Molybdenum Oxide/Pt-black Composite

Author: Fan Yang Fan Li Yan Wang Xin Chen Dingguo Xia  
Jingbo Liu



PII: S1381-1169(15)00049-7  
DOI: <http://dx.doi.org/doi:10.1016/j.molcata.2015.02.001>  
Reference: MOLCAA 9417

To appear in: *Journal of Molecular Catalysis A: Chemical*

Received date: 2-9-2014  
Revised date: 25-1-2015  
Accepted date: 1-2-2015

Please cite this article as: Fan Yang, Fan Li, Yan Wang, Xin Chen, Dingguo Xia, Jingbo Liu, Enhanced Electrocatalytic Performance for Methanol Oxidation with a Magnéli Phase Molybdenum Oxide/Pt-black Composite, *Journal of Molecular Catalysis A: Chemical* <http://dx.doi.org/10.1016/j.molcata.2015.02.001>

This is a PDF file of an unedited manuscript that has been accepted for publication. As a service to our customers we are providing this early version of the manuscript. The manuscript will undergo copyediting, typesetting, and review of the resulting proof before it is published in its final form. Please note that during the production process errors may be discovered which could affect the content, and all legal disclaimers that apply to the journal pertain.

## Enhanced Electrocatalytic Performance for Methanol Oxidation with a Magnéli Phase Molybdenum Oxide/Pt-black Composite

Fan Yang<sup>a</sup>, Fan Li<sup>a\*</sup>, Yan Wang<sup>a,b</sup>, Xin Chen<sup>a</sup>, Dingguo Xia<sup>c\*</sup>, Jingbo Liu<sup>d\*</sup>

(a. Department of Chemistry and Chemical Engineering, Beijing University of Technology, Ping le yuan 100, 100124, Beijing, China. E-mail: vanadiumli@bjut.edu.cn;

b. National Engineering Laboratory for Advanced Coatings Technology of Metal Material, China Iron and Steel Research Institute Group, 100081, Beijing, China

c. College of Engineering, Peking University, Beijing 100871, China. E-mail: dgxia@pku.edu.cn

d. Department of Chemistry, Texas A&M University-Kingsville, Kingsville, Texas 78363, E-mail: Highlights ▶ jingbo.liu@chem.tamu.edu)

Highlights

### Enhanced Electrocatalytic Performance for Methanol Oxidation with a Magnéli Phase Molybdenum Oxide/Pt-black Composite

1. Crystallised Magnéli phase Mo<sub>4</sub>O<sub>11</sub> used as a co-catalyst support to enhance MOR
2. Multiple Mo valence states coexist in Mo<sub>4</sub>O<sub>11</sub>
3. These promote hydrogen spillover and oxygen buffering in the Pt/Mo<sub>4</sub>O<sub>11</sub> catalyst.
4. The catalyst shows improved poisoning tolerance and electrocatalytic activity.

Graphical abstract **Enhanced Electrocatalytic Performance for Methanol**

### Oxidation with a Magnéli Phase Molybdenum Oxide/Pt-black Composite

Abstract

A composite electrocatalyst composed by prepared Magnéli phase Mo<sub>4</sub>O<sub>11</sub> and Pt-black (Pt/Mo<sub>4</sub>O<sub>11</sub>) was found with highly effective for the methanol oxidation reaction (MOR). Cyclic voltammetry (CV) result showed that the mass activity for the forward peak (I<sub>f</sub>) of Pt/Mo<sub>4</sub>O<sub>11</sub> was determined to be 722.20 mA·mg<sup>-1</sup><sub>Pt</sub>, e.g., about twice of the mass activity of the stand-alone Pt-black. This suggested that the electrocatalytical reactivity is improved when the crystallised Mo<sub>4</sub>O<sub>11</sub> assists for methanol oxidation. It is also found that the peak current ratio of the forward versus the reverse (I<sub>f</sub>/I<sub>b</sub>) is 1.21 for Pt/Mo<sub>4</sub>O<sub>11</sub> and 0.81 for Pt/C, respectively. X-ray photoelectron spectroscopy (XPS) results indicated that different valence states of molybdenum coexist in Mo<sub>4</sub>O<sub>11</sub>; this promotes both hydrogen spillover and oxygen buffering effects. The synergistic effects of Pt and Mo<sub>4</sub>O<sub>11</sub> on the electrochemical properties represent a critical advantage of the Pt/Mo<sub>4</sub>O<sub>11</sub> catalyst for anti-poisoning towards the intermediates in the MOR.

**Keywords:** crystallised Magnéli phase,  $\text{Mo}_4\text{O}_{11}$ , methanol oxidation reaction, poisoning tolerance

## 1 Introduction

Diversified energetic resources, growth in generation capacity, and feasible strategies are required to meet the increasing energy needs of our society [1-2]. One promising alternative strategy is to use fuel cells as green energy sources to spontaneously convert chemical energy into electricity, releasing heat and water when the electrochemical reactions occur [3-4]. Direct methanol fuel cells (DMFCs), which use liquid and renewable methanol as fuel supplies, have recently received much attention by the scientific community. The advantages of DMFCs over hydrogen-fed fuel cells include convenient storage and transportation of fuels, high specific energy density at low operating temperature, and flexible design of the fuel cell devices [1-3]. However, several issues hinder their commercialization, such as durability, efficiency, and costs. One of the major difficulties is the sluggish kinetics for the methanol oxidation reaction (MOR) of the most commonly used Pt-anode catalysts in DMFCs; this is the result of the self-poisoning caused by strongly adsorbed intermediates such as CHO and CO, ect.. [4-8]. In order to address this critical issue, in the last decade different kinds of co-catalytic elements, such as Ru, Ce, and W, have been incorporated into the Pt-based catalysts [9-14]. The presence of second and/or third elements in the Pt-based catalysts may improve the MOR kinetics via a bifunctional mechanism or a synergistic effect.

Numerous studies have shown that Mo-modified Pt electrocatalysts possess effective poisoning tolerance towards MOR. Ross and his co-workers [15,16] confirmed that PtMo alloys have exceptional low-temperature CO-tolerance in bulk electrodes. However, synthesis of PtMo nanoparticles is particularly challenging, because of the large negative redox potential of the  $\text{Mo}^{\text{n+}}/\text{Mo}^0$  couple and the low miscibility of Pt and Mo. Yet, Pt catalysts modified by molybdenum oxides (instead of simple Mo) displayed high tolerance toward CO [17-19]. Although  $\text{MoO}_x$  is an effective co-catalyst owing to the several accessible valence states of Mo (IV, V, and VI), its

amorphous characteristics lead to poor conductivity [20]. To solve this issue,  $\text{MoO}_x$  particles have been deposited on carbon-based materials such as carbon black, carbon nanotubes, or carbon nanofibers [21-23]. To date, co-depositions [24] and consecutive impregnations [25] have been developed to prepare Pt/ $\text{MoO}_x$ /C catalysts. However, a certain amount of Pt is embedded and capped as a result of these methods; this problem reduces their applicability. New approaches that improve the conductivity of Mo oxides are thus highly desired. For instance, it was found that a sub-stoichiometric compound in MoO systems (e.g., the Magnéli phase) has a suitable electronic conductivity. Among these Mo oxides,  $\text{Mo}_4\text{O}_{11}$  has received much attention because of its quasi-two-dimensional [26,27]; for instance, electrical resistivity of  $\gamma$ - $\text{Mo}_4\text{O}_{11}$  single crystals is about  $10^{-6} \Omega\cdot\text{m}$  at 300 K [28]. Based on the results of our previous study on Magnéli phase  $\text{Ti}_4\text{O}_7$  as a novel durable Pt catalyst support [29], we further showed in this study that the electron conductor Magnéli phase  $\text{Mo}_4\text{O}_{11}$  can be employed as a co-catalyst support, with a high poisoning tolerance. In particular, electrochemical tests indicated that crystallised  $\text{Mo}_4\text{O}_{11}$  mixed with Pt-black shows improved anti-poisoning for the intermediates in the MOR. Results based on X-ray photoelectron spectroscopy (XPS) also suggested that a strong metal-support interaction occurs between Pt and  $\text{Mo}_4\text{O}_{11}$ , and that different valence states of molybdenum (IV, V, and VI) coexist in  $\text{Mo}_4\text{O}_{11}$ . This is a favourable feature that can promote hydrogen spillover and oxygen buffering effects, which may contribute to improve the anti-poisoning properties and the electrocatalytic activity of the Pt/ $\text{Mo}_4\text{O}_{11}$  catalyst. The synergistic effect of the Pt/  $\text{Mo}_4\text{O}_{11}$  catalyst and a possible mechanism of the catalytic process were also studied and discussed in detail.

## 2 Experimental

### 2.1 Synthesis of the $\text{Mo}_4\text{O}_{11}$ support

All reagents were of analytical grade and used as received without further purification. In a typical procedure, the  $\text{Mo}_4\text{O}_{11}$  support was synthesised *via* two steps. Firstly, the  $\text{MoO}_3$  precursor was obtained as follows: 15 g of  $(\text{NH}_4)_6\text{Mo}_7\text{O}_{24}\cdot 4\text{H}_2\text{O}$  (AMT) was dispersed in an alumina ceramic boat and placed in a tube furnace in ambient

atmosphere; the temperature was then raised to 873 K with a rate of 5 K·min<sup>-1</sup>, and kept constant for 5 h; finally, the system was naturally cooled to room temperature. Secondly, 5 g of the MoO<sub>3</sub> precursor was reduced in a H<sub>2</sub> (5 vol%)-Ar mixing-gas flow at 873 K for 4 h to synthesise the Mo<sub>4</sub>O<sub>11</sub> support. To load the Pt nanoparticles on the Mo<sub>4</sub>O<sub>11</sub> support, 20 mg of Pt-black and 80 mg of the as-synthesised Mo<sub>4</sub>O<sub>11</sub> support were mechanically mixed for 0.5 h.

## 2.2 Characterizations of materials

The crystalline phases of the MoO<sub>3</sub> precursor and Mo<sub>4</sub>O<sub>11</sub> were characterised by X-ray powder diffraction (XRD) analysis (D8 Advance, Bruker, Karlsruhe, Deutschland). Morphologies were observed using a scanning electron microscope (SEM, Hitachi S-4300, Tokyo, Japan). Transmission electron microscopy (TEM) and high-resolution transmission electron-microscopy (HRTEM) images of Pt/Mo<sub>4</sub>O<sub>11</sub> were taken by a JEOL JEM2100 (TEM, JEOL JEM2100, Tokyo, Japan). Surface properties and the electronic structure of the catalysts were evaluated by XPS with Al K<sub>α</sub> radiation (Kratos AXIS Ultra DLD, Manchester Britain). The binding energy was calibrated with the C1s position of the carbon support at 284.80 eV. The composition of the catalysts was determined by inductively coupled plasma atomic-emission spectrometry (ICP-AES, Thermo Fisher, IRIS Intrepid ER/S, Waltham, USA).

## 2.3 Electrochemical measurements

Glassy carbon (GC) electrodes were polished with alumina powder, ultrasonic washing and blow drying, before dropping the catalyst ink. Based on the ICP-AES measurements, Pt/Mo<sub>4</sub>O<sub>11</sub> and Pt-black (Hispec 1000, Johnson Matthey) were diluted to 1.3 mg·mL<sup>-1</sup> and 0.8 mg·mL<sup>-1</sup> with 0.05 wt% ethanol diluted Nafion solution, respectively. Then, 10 μl of the two suspensions were transferred onto the polished GC electrode substrates. Before testing, the electrodes were solidified for 0.5 hours under ambient conditions.

Electrochemical measurements were performed by cyclic voltammogram (VMP3, Bio-Logic SA). The GC electrode (Ø5 mm, with an area of 0.196 cm<sup>2</sup>) was set as the working electrode. A Pt foil (10×10×0.3 mm) and a reversible hydrogen electrode (RHE) were used as the counter electrode and the reference electrode, respectively.

The RHE was filled with 0.1 M HClO<sub>4</sub> solution. Cyclic voltammetry (CV) measurements were carried out in an Ar-purged 0.1 M HClO<sub>4</sub> solutions at a sweep rate of 100 mV·s<sup>-1</sup>. The electrochemically active surface area (ECSA) was calculated based on equation (1), as follows:

$$ECSA = \frac{Q_H}{0.21[Pt]} \quad (1)$$

where the correlation constant of 0.21 (mC·cm<sup>-2</sup>) represents the charge required for the monolayer adsorption of hydrogen on a Pt surface. [Pt] is the Pt loading (mg·cm<sup>-2</sup>) on the electrode,  $Q_H$  is the amount of charge exchanged during the adsorption of hydrogen atoms on Pt (mC·cm<sup>-2</sup>), which measured under the electro-adsorption curves between 0.05 V and 0.4 V.

MOR measurements were performed in a 0.1 M HClO<sub>4</sub> and 0.1 M CH<sub>3</sub>OH solution at a sweep rate of 100 mV·s<sup>-1</sup> under ambient atmosphere. Durability tests (DTs) were performed in an Ar-purged 0.1 M HClO<sub>4</sub> solution at a sweep rate of 100 mV·s<sup>-1</sup> for 1500 cycles.

### 3 Results and discussion

#### 3.1 Crystalline phase analysis

Morphologies and crystal structures of the MoO<sub>3</sub> precursor and of the synthesised Mo<sub>4</sub>O<sub>11</sub> support are shown in Fig. S1. In particular, XRD data (Fig. S1B) indicated that MoO<sub>3</sub> has an orthorhombic crystalline structure and that is well-indexed with the standard profiles (PDF 35-0609). The molybdenum suboxide Mo<sub>4</sub>O<sub>11</sub> (Fig. S1D) was formed in the reducing atmosphere at the temperature of 873 K, and it consists of a mixture of monoclinic and orthorhombic phases (at 2θ of 22°). The principal phase of orthorhombic was well-indexed with the standard profiles (PDF 05-0338). In line with previous studies [30,31], about 8.7 (wt.) % of MoO<sub>2</sub> was found in the as-synthesised of Mo<sub>4</sub>O<sub>11</sub> (Fig. 1A). It was also found that the orthorhombic phase transforms into the monoclinic phase when kept for a relatively long time at high temperatures (such as 873 K), while the orthorhombic phase is thermodynamically stable at temperatures

higher than 1000 K. In order to prevent agglomeration of  $\text{MoO}_3$  particles during the high-temperature reduction and to improve the purity of the  $\text{Mo}_4\text{O}_{11}$  product will be systematically investigated in future. As shown in Fig. 1B, both  $\text{Mo}_4\text{O}_{11}$  and Pt were detected when the electrocatalyst Pt/ $\text{Mo}_4\text{O}_{11}$  was investigated with XRD. Pt displayed a face-centred cubic and was indexed with the standard (PDF 04-0802). Because the size of Pt-black is significantly smaller than that of micro-sized  $\text{Mo}_4\text{O}_{11}$ , Pt/ $\text{Mo}_4\text{O}_{11}$  shows the electronic-conductor Magnéli phase  $\text{Mo}_4\text{O}_{11}$  decorated by Pt-black (Fig. 1B).

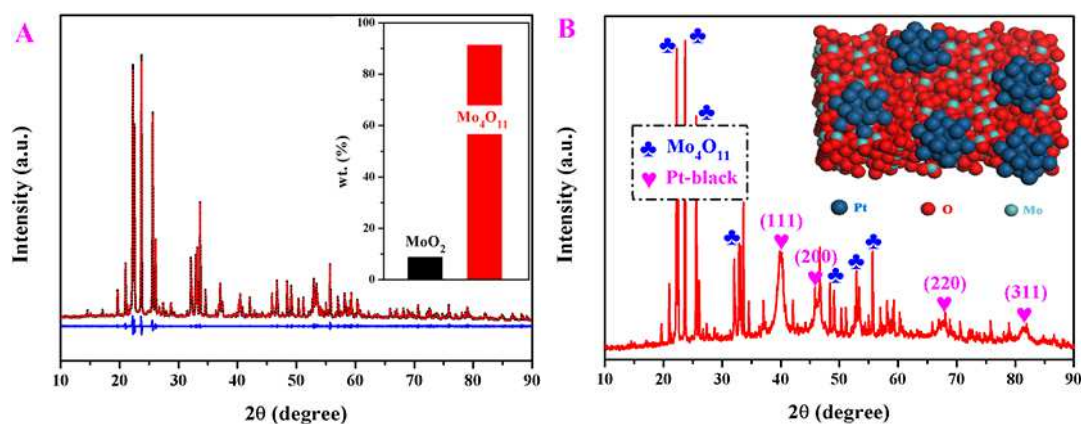
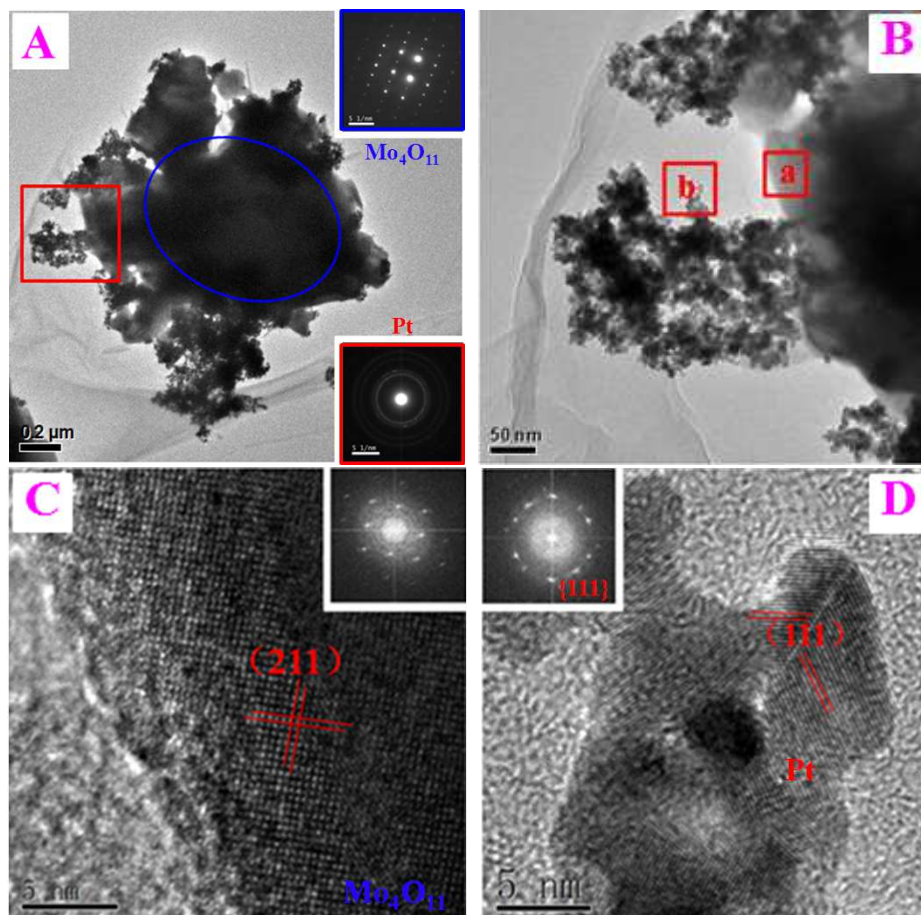


**Fig. 1** (A) Quantitative fit analysis of  $\text{Mo}_4\text{O}_{11}$  by MDI Jade program; phases content is shown in the inset. (B) X-ray powder diffraction (XRD) patterns of Pt/ $\text{Mo}_4\text{O}_{11}$  and the atomic schematic graph shown in the inset.

### 3.2 Morphological analysis

The TEM micrograph (Fig. 2) confirmed that Pt-black is deposited on the surface of the Magnéli phase  $\text{Mo}_4\text{O}_{11}$ . Orderly dispersed points were observed by the selected area electron diffraction (SAED) pattern of the blue core region (Fig. 2A), indicating, in line with the XRD data, the formation of a monoclinic  $\text{Mo}_4\text{O}_{11}$ . In contrast, ring patterns of the small particles were collected in the SAED (Fig. 2A), which are indexed as (111), (200), (220), and (311) planes of the face-centred-cube (*fcc*) of the Pt crystal. This finding suggested that the core  $\text{Mo}_4\text{O}_{11}$  is decorated by the Pt-black particles, in agreement with the XRD results (Fig. 1B). To further investigate the bonding between  $\text{Mo}_4\text{O}_{11}$  and Pt-black, high-magnification TEM and HRTEM were employed. Fig. 2B displays an enlarged image of the area marked in Fig. 2A, which clearly shows that the Pt-black nanoparticles are dispersedly attached on the surface

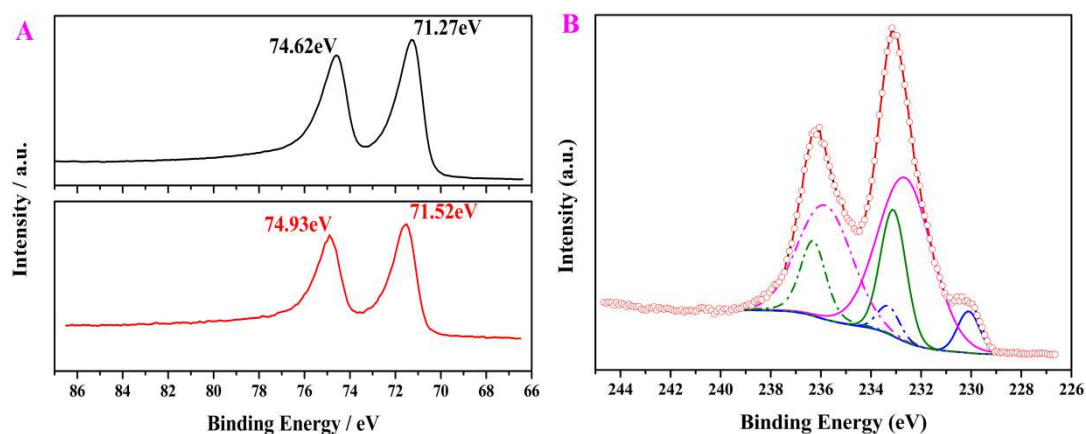
of  $\text{Mo}_4\text{O}_{11}$ ; Fig. 2C displays the HRTEM image of the marked  $\text{Mo}_4\text{O}_{11}$  area (region “a” in Fig. 2B), which indicates that the  $\text{Mo}_4\text{O}_{11}$  (211) lattice plane is exposed. The Fourier transform (FT) pattern (inset in Fig. 2C) further proved this observation. Fig. 2D shows the HRTEM image of marked Pt-black area (region “b” in Fig. 2B), showing that the Pt (111) lattice plane is exposed. Previous studies showed that the Pt (111) lattice plane of Pt exhibits highly electrocatalytic activity [32,33].



**Fig. 2** (A) Transmission electron microscopy (TEM) image of Pt/ $\text{Mo}_4\text{O}_{11}$  and the selected area electron diffraction (SAED) pattern are shown in the inset, up-right (blue area) is the monoclinic  $\text{Mo}_4\text{O}_{11}$  and down-right (red area) is the Pt-black, respectively; (B) high-magnification TEM image of the area marked with a red square in Fig. 2A; (C) high-resolution transmission electron-microscopy (HRTEM) image of the marked  $\text{Mo}_4\text{O}_{11}$  area (a in Fig. 2B), with a Fourier transform (FT) pattern shown in the inset; (D) HRTEM image of the marked Pt-black area (b in Fig. 2B), with a FT pattern shown in the inset.

### 3.3 Oxidation state analysis

XPS measurements were performed to examine the composition of Pt/Mo<sub>4</sub>O<sub>11</sub> and Pt-black as well as the valence state of the metal elements. The Pt 4f spectra of Pt/Mo<sub>4</sub>O<sub>11</sub> and Pt-black are shown in Fig. 3A. Comparison of these spectra suggested that the binding energy of Pt 4f for Pt/Mo<sub>4</sub>O<sub>11</sub> depends on the blue shifts (71.52eV), indicating that an interaction between Pt and the Mo<sub>4</sub>O<sub>11</sub> support exists. This shift may be regarded as a strong metal-support interaction effect [19,29]. This strong interaction may promote the mass transfer between Pt-black and Mo<sub>4</sub>O<sub>11</sub>, which in turn may enhance the catalytic activity of the catalyst. Fig. 3B displays the results of the deconvolution of Mo 3d peaks of the Mo<sub>4</sub>O<sub>11</sub> support. The Mo 3d<sub>5/2</sub> signals at 230.11, 232.66, and 233.11 eV are assigned to Mo(IV), Mo(V), and Mo(VI), respectively. Our results thus indicate that different states of Mo 3d are coexisting in Mo<sub>4</sub>O<sub>11</sub>. The presence of multiple valence could promote hydrogen spillover and oxygen buffering effects, which may contribute to the improvement of the intermediate-tolerance and electroactivity of the Pt/Mo<sub>4</sub>O<sub>11</sub> catalyst. Although peaks of the binding energy and intensities of peaks of Mo 3d for Pt/Mo<sub>4</sub>O<sub>11</sub> significantly changed before (Fig. 3C) and after (Fig. 3D) the durability tests, these spectra were found to correlate with Mo(IV), Mo(V), Mo(VI) states. The deconvolution statistics (Table S1) confirmed that synergistic effects occurred in the Pt/Mo<sub>4</sub>O<sub>11</sub> composite.



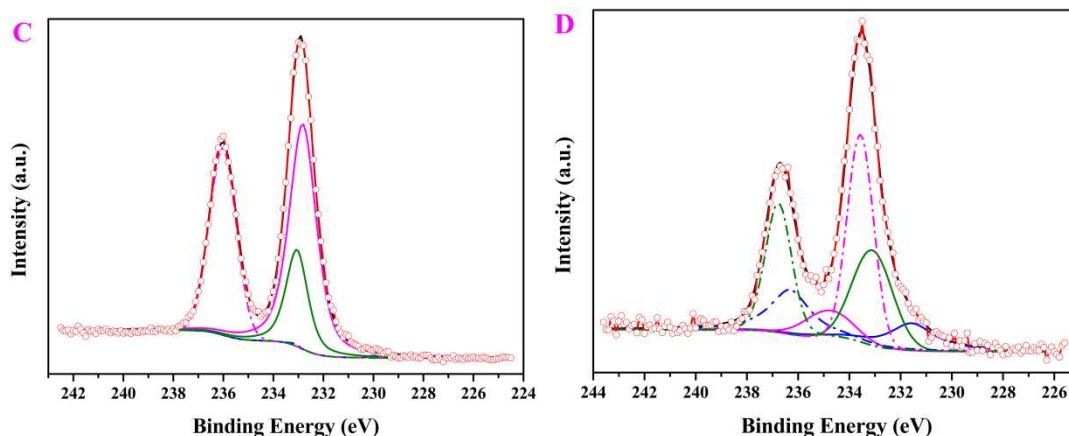
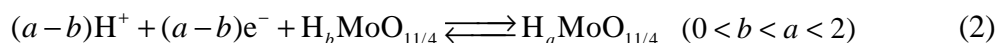


**Fig. 3** (A) X-ray photoelectron spectroscopy (XPS) spectra of Pt 4f for Pt/Mo<sub>4</sub>O<sub>11</sub> (red) and Pt-black (black); (B) Mo 3d spectra for the Mo<sub>4</sub>O<sub>11</sub> support; Mo 3d spectra of Pt/Mo<sub>4</sub>O<sub>11</sub> before (C) and after (D) the durability tests.

### 3.4 Electrochemical behaviour of Pt/Mo<sub>4</sub>O<sub>11</sub>

According to previous studies [15,18], metallic molybdenum or molybdenum oxide-modified Pt catalysts have shown enhanced CO-tolerance for the MOR. Fig. 4A displays CV curves of Pt/Mo<sub>4</sub>O<sub>11</sub> and Pt-black recorded at ambient conditions in an Ar-purged 0.1 M HClO<sub>4</sub> solution. The ECSA of the Pt/Mo<sub>4</sub>O<sub>11</sub> catalyst was calculated *via* equation (1) to be 40.05 m<sup>2</sup>·g<sup>-1</sup> (Fig. S2), e.g., 1.62 times larger than that of Pt-black (24.73 m<sup>2</sup>·g<sup>-1</sup>). However, Mo<sub>4</sub>O<sub>11</sub> has no obvious absorption and desorption of hydrogen region (Fig. S3A), the ECSA of Mo<sub>4</sub>O<sub>11</sub> is negligible compared with that of Pt/Mo<sub>4</sub>O<sub>11</sub> (Fig. S3B). These results indicated that the main role of Mo<sub>4</sub>O<sub>11</sub> is that of improving the distribution and the activity of Pt: On one hand, Mo<sub>4</sub>O<sub>11</sub> acts as the carbonaceous support to attach Pt-black nanoparticles and to increase the electrochemically active sites, on the other hand, the hydrogen spillover effects may occur on the Mo<sub>4</sub>O<sub>11</sub> support, due to the presence of the metal, which serves as a lower-energy pathway for H<sub>2</sub> to firstly adsorb onto the metal and then diffuse on the support surface. As shown in Fig. 4, clear redox peaks of MoO<sub>x</sub> between 0.35 V and 0.55 V were detected. These were attributed to the Faradaic process of intercalation/de-intercalation of hydrogen into MoO<sub>x</sub>, forming hydrogen molybdenum bronzes, e.g., H<sub>a</sub>MoO<sub>x</sub> (0 < a < 2) [34-37]. The stoichiometric formula can be depicted as MoO<sub>11/4</sub>, where the hydrogen spillover occurs on the surface of the H<sub>a</sub>MoO<sub>x</sub>, as in

equation (2).



We suggest for steps for the hydrogen spillover effect (Fig. 4A): i), reactant molecules, such as  $\text{H}_2$  and  $\text{CH}_3\text{OH}$ , are chemically adsorbed on the Pt surface and then dissociated to hydrogen atoms (H); ii), hydrogen atoms are oxidised to cation, providing an extra electron for  $\text{MoO}_{11/4}$ ; iii),  $\text{H}^+$  is transferred to the  $\text{MoO}_{11/4}$  surface by a spillover mechanism; iv)  $\text{H}^+$  diffuses into the  $\text{MoO}_{11/4}$  lattice, reacting with the electron and the matrix to neutralise the charge, this leading to the formation of  $\text{H}_a\text{MoO}_{11/4}$ . Thus, both the enhanced dispersion by the  $\text{Mo}_4\text{O}_{11}$  support and the hydrogen spillover on the surface of  $\text{H}_a\text{MoO}_{11/4}$  improved the ECSA of  $\text{Pt}/\text{Mo}_4\text{O}_{11}$  catalyst.

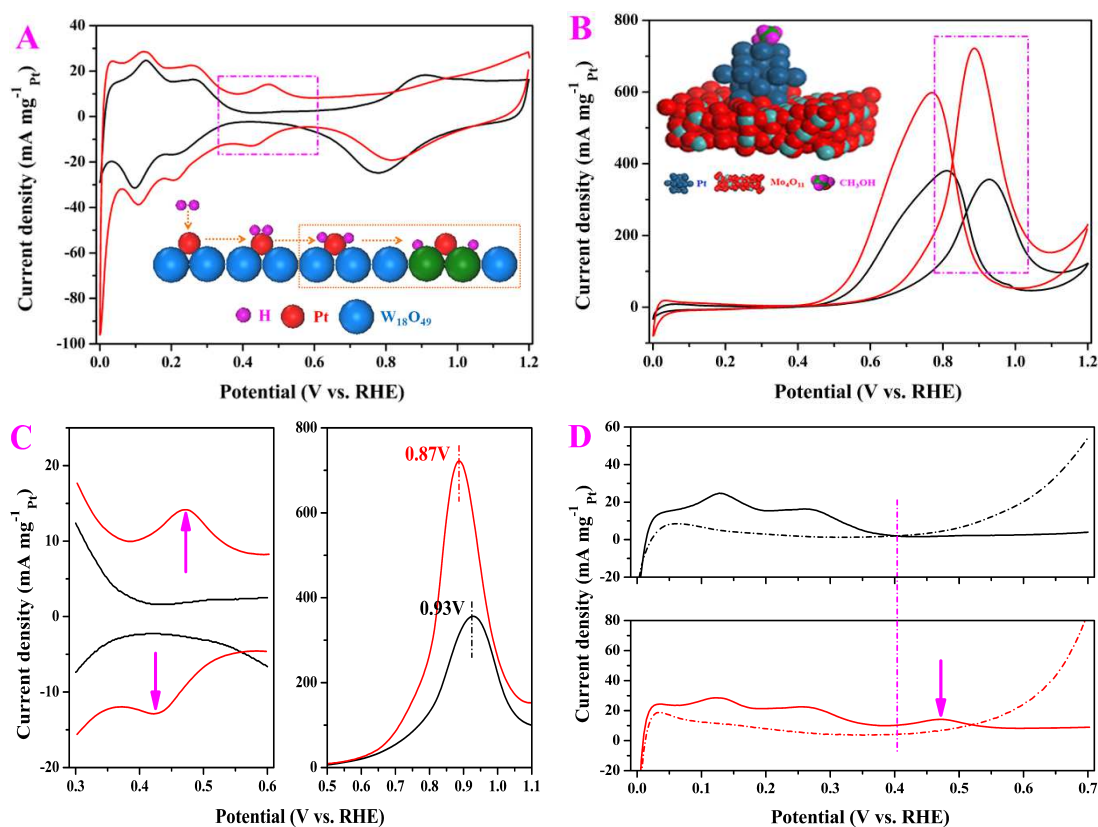


**Fig.4** Comparison of the electrocatalytic activities of  $\text{Pt}/\text{Mo}_4\text{O}_{11}$  and Pt-black. Pt loading was 2.6 and 8  $\mu\text{g}$  for  $\text{Pt}/\text{Mo}_4\text{O}_{11}$  and Pt-black, respectively. (A) CV curves recorded in an Ar-purged 0.1 M  $\text{HClO}_4$  solution with a sweep rate of  $100 \text{ mV}\cdot\text{s}^{-1}$  of  $\text{Pt}/\text{Mo}_4\text{O}_{11}$  (red) and Pt-black (black), as well as a schematic illustration of hydrogen spillover effect shown in inset, the green ball ( $\text{MoO}_{11/4}$ ) with the violate ball (H)

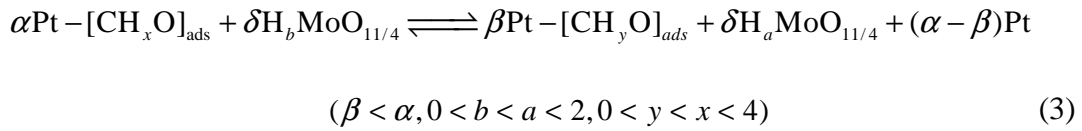
together to form hydrogen molybdenum bronzes,  $H_aMoO_{11/4}$ ; (B) CV curves recorded in a 0.1 M  $HClO_4$  and 0.1 M  $CH_3OH$  mixed solution at a sweep rate of  $100\text{ mV}\cdot\text{s}^{-1}$  under ambient atmosphere, and a schematic of methanol adsorption shown in the inset; (C) enlarged images of the purple squares in Fig. 4A (left) and Fig. 4B (right), respectively; (D) enlarged images of the CVs (solid) and MOR CVs (dash) between 0 V and 0.7 V.

### 3.5 Comparison of Pt/Mo<sub>4</sub>O<sub>11</sub> and Pt-black behaviour

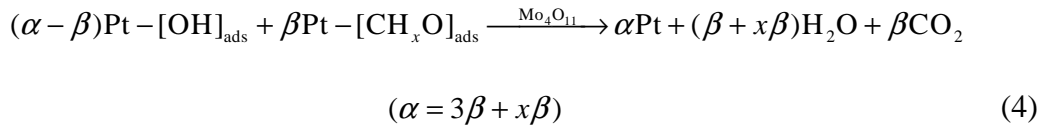
MoO<sub>x</sub> materials have recently received much attention, due to their high oxygen storage capacity, similar to that of CeO<sub>x</sub> [38]. Enhancement of the utilization and stability of Pt catalyst activity with these series of oxides is critical for MOR. Crystallised MoO<sub>11/4</sub> becomes an option because of its intrinsic properties, i.e., the high electronic conductivity and the oxygen buffering effect [22,39]. Redox couples in different valence states of molybdenum can facilitate oxygen transfer to the interface between Pt and MoO<sub>11/4</sub>. The CV curves of MOR for Pt/Mo<sub>4</sub>O<sub>11</sub> and Pt-black (Fig. 4B) showed that the forward peak current ( $I_f$ ) of Pt/Mo<sub>4</sub>O<sub>11</sub> ( $722.20\text{ mA}\cdot\text{mg}^{-1}_{Pt}$ ) is 2.03 times larger than that of Pt-black ( $356.10\text{ mA}\cdot\text{mg}^{-1}_{Pt}$ ). The forward peak potential ( $F_p$ ) of Pt/Mo<sub>4</sub>O<sub>11</sub> was found to be shifted to a lower value (0.87 V), compared with the potential of Pt-black (0.93V). The ratio of the forward peak current to the back peak current ( $I_f/I_b$ ) is 1.21 for Pt/Mo<sub>4</sub>O<sub>11</sub>, 0.94 for Pt-black, and 0.81 for Pt/C (Fig. S4),. These data indicated that Pt-black mixed with crystallised Mo<sub>4</sub>O<sub>11</sub> has a higher poisoning tolerance than that of the Pt-black and Pt/C catalysts. The peak potentials and currents of the MOR on the electrodes (Table S2) suggested that the Pt/Mo<sub>4</sub>O<sub>11</sub> can provide comparable electrochemical reactivity as that of the Pt/C catalyst. Thus, it can be concluded that the Pt/Mo<sub>4</sub>O<sub>11</sub> catalysts are characterised by an improved tolerance to CO poison.

Fig. 4D shows the comparison between the CVs (solid) and MOR CVs (dash) for Pt/Mo<sub>4</sub>O<sub>11</sub> and Pt-black, with an applied voltage ranging between 0.0 V and 0.7 V. Although the onset potential of Pt/Mo<sub>4</sub>O<sub>11</sub> is equivalent to that of Pt-black, the  $I_f$  value of Pt/Mo<sub>4</sub>O<sub>11</sub> is higher than that of Pt-black, this suggests that the kinetics of MOR reaction catalysed by Pt/Mo<sub>4</sub>O<sub>11</sub> are more effective; in contrast, the  $I_f$  potential of

Pt/Mo<sub>4</sub>O<sub>11</sub> is lower than that of Pt-black, which shows that Pt/Mo<sub>4</sub>O<sub>11</sub> catalytic dehydrogenation of methanol are thermodynamically easier. This observation may be attributed to the intense dehydrogenation from methanol occurring after de-intercalation on the surface of H<sub>a</sub>MoO<sub>11/4</sub>. In particular, the I<sub>f</sub> value results from the methanol adsorption on the surface of Pt, followed by the dehydrogenation reaction. Hydrogen intercalation/de-intercalation on the surface of Mo<sub>4</sub>O<sub>11</sub>, (H<sub>b</sub>MoO<sub>11/4</sub> ↔ H<sub>a</sub>MoO<sub>11/4</sub>) plays an essential role in the removal of a certain amount of produced intermediate poisonous substances from the surface of Pt; more hydrogen de-intercalation from H<sub>a</sub>MoO<sub>11/4</sub> results in more hydrogen dissociated from methanol adsorbed on Pt. This process can be described with the following equation (3), its schematic demonstration being shown in Fig. 5I:



The dissociated hydrogen can be embedded into H<sub>b</sub>MoO<sub>11/4</sub> to form H<sub>a</sub>MoO<sub>11/4</sub> by the hydrogen spillover effect, releasing (α-β) Pt active sites. As the reaction proceeds, oxygen rapidly diffuses and binds to the surface of the (α-β) Pt active sites to form Pt-O<sub>ads</sub> species, *via* an oxygen buffering effect of the Mo<sub>4</sub>O<sub>11</sub> support. The formation of Pt-O<sub>ads</sub> in turn promotes the oxidization of β Pt-[CH<sub>y</sub>O]<sub>ads</sub> to H<sub>2</sub>O and CO<sub>2</sub>, and regeneration of free Pt sites for further oxidation of methanol. This also explains the highly anti-poisoning (removal the adsorbed intermediate product) property of Pt/Mo<sub>4</sub>O<sub>11</sub>. This process can be described with the following equation (4), its schematic demonstration being shown in Fig. 5II:



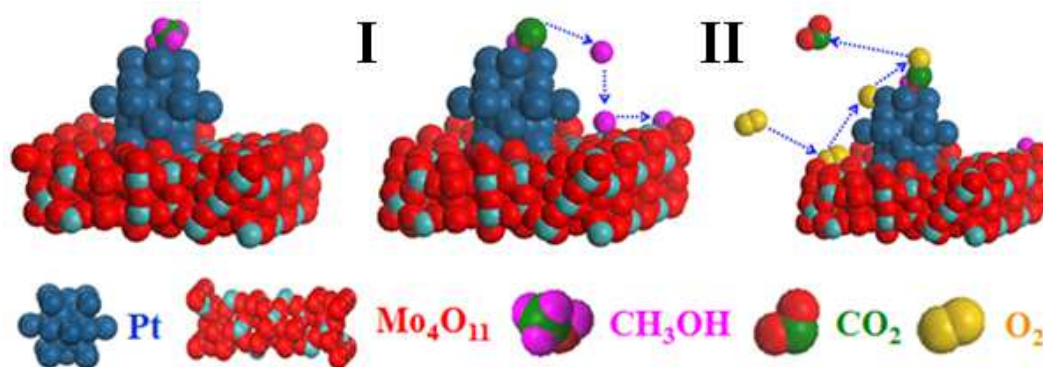


**Fig. 5** Schematic illustration of methanol oxidation reaction on the Pt/Mo<sub>4</sub>O<sub>11</sub> catalyst; I and II represent the hydrogen spillover effect, and the oxygen buffering effect, respectively.

### 3.6 Stability of the electrocatalysts

Stability is a critical criterion to evaluate the performance of an electrocatalyst. The DTs were estimated by CV sweeps at  $100 \text{ mV}\cdot\text{s}^{-1}$  in an Ar-purged 0.1 M HClO<sub>4</sub> solution at room temperature (Fig. S5). The ECSAs of Pt-black and Pt/Mo<sub>4</sub>O<sub>11</sub> are reduced with the increment of the CV circles, as shown in Figures S5A and S5B, respectively. After 500 cycles, the loss rate of Pt-black was found to be 16.91% (to compare with 8.93% of Pt/Mo<sub>4</sub>O<sub>11</sub>). The ECSA loss of the Pt-black was attributed to the aggregation of the nanoparticles during the test and it may be explained as follows: the Pt is separated from the surface of support during preparation, because of the mechanical mixing and the solubility of hydrogen molybdenum bronzes after Mo<sub>4</sub>O<sub>11</sub> intercalation of hydrogen. The molybdenum dissolution can be detected *via* the colour change of the supernatant (composed of H<sub>8</sub>MoO<sub>11/4</sub>) to blue (Fig. S6). To further illustrate the presence of soluble molybdenum bronzes, we performed accelerated DTs by increasing the CV scanning potential range, between 0.0 V and 1.2V (Fig. S7). The XRD results (Fig. S8) showed that the relative intensity ratio of Pt to Mo<sub>4</sub>O<sub>11</sub> increases significantly after 1500 cycles of the DT. This may result from the loss of Mo<sub>4</sub>O<sub>11</sub> during the process. Therefore, we suggest that the degeneration of ECSA of Pt/Mo<sub>4</sub>O<sub>11</sub> is related to the instability of Mo<sub>4</sub>O<sub>11</sub>.

Although the mechanical mixing showed some limitations in the effective dispersion of Pt on the surface of Mo<sub>4</sub>O<sub>11</sub>, the ECSA of Pt/Mo<sub>4</sub>O<sub>11</sub> is 1.62 times larger

than that of Pt-black. Even after 1500 cycles of DT, the ECSA obtained from the CV curve of Pt/Mo<sub>4</sub>O<sub>11</sub> (26.28 m<sup>2</sup>·g<sup>-1</sup>) hardly changed from that of Pt-black (24.73 m<sup>2</sup>·g<sup>-1</sup>) before DT. This demonstrates the evident advantages of using the co-catalyst support composed of crystallised Mo<sub>4</sub>O<sub>11</sub> over traditional catalysts. Although methods for an efficient Pt loading need to be developed, our data showed that Pt/Mo<sub>4</sub>O<sub>11</sub> displays a reasonably high electrochemical activity for MOR. Despite the formation of hydrogen molybdenum bronzes accelerated the ECSA loss of Pt/Mo<sub>4</sub>O<sub>11</sub>, it also promoted hydrogen spillover and oxygen buffering effect, which may contribute to improve the poisoning tolerance and electrocatalytic activity of the Pt/Mo<sub>4</sub>O<sub>11</sub> catalyst towards MOR.

#### **4 Summary**

In this work, crystallised Magnéli phase Mo<sub>4</sub>O<sub>11</sub> as a quasi-two-dimensional conductor has been used as a co-catalyst support, mixed with Pt-black to enhance MOR. XPS results revealed a strong metal-support interaction between the Pt and Mo<sub>4</sub>O<sub>11</sub>; in addition, various valence states of Mo (IV, V, and VI) were found to coexist in Mo<sub>4</sub>O<sub>11</sub>, which may promote hydrogen spillover and oxygen buffering. These effects together contributed to the improvement of the poisoning tolerance and the electrocatalytic activity of the Pt/Mo<sub>4</sub>O<sub>11</sub> catalyst for MOR. Thus, the results collected in this work demonstrated that the crystallised Magnéli phase Mo<sub>4</sub>O<sub>11</sub> may be regarded as a promising co-catalyst support for MOR. Further studies are needed to improve the stability of the crystallised Magnéli phase Mo<sub>4</sub>O<sub>11</sub>, which is a critical property for the performance of an electrocatalyst.

#### **Acknowledgment**

The authors gratefully acknowledge Prof. Jiwu Huang (Central South University) for his assistance in the quantitative analysis by JADE. This work was financially supported by National Natural Science Foundation of China (51172007, 11179001, 50974006), Beijing Municipal Natural Science Foundation (2120001, 2110001, 2102004), and the Funding Project for Academic Human Resources Development in Institutions of Higher Learning under the jurisdiction of the Beijing Municipality (PHR 201107104).

## References

- [1] M. Winter and R. J. Brodd. What Are Batteries, Fuel Cells, and Supercapacitors?. *Chem. Rev.* 2004;104:4245-4269.
- [2] E. Antolini, J. R. C. Salgado and E. R. Gonzalez. The methanol oxidation reaction on platinum alloys with the first row transition metals The case of Pt–Co and –Ni alloy electrocatalysts for DMFCs: A short review. *Appl. Catal. B: Environ.* 2006;63:137-149.
- [3] S. K. Kamarudin, F. Achmad and W. R. W. Daud. Overview on the application of direct methanol fuel cell (DMFC) for portable electronic devices *Int. J. Hydrogen Energy* 2009;34:6902-6916.
- [4] B. Beden, C. Lamy, A. Bewick and K. Kunimatsu. Electrosorption of Methanol on a Platinum Electrode IR Spectroscopic Evidence for Adsorbed Species. *J. Electroanal. Chem. Interfacial Electrochem.* 1981;121:343-347.
- [5] H. Igarashi, T. Fujino and M. Watanabe. Hydrogen electro-oxidation on platinum catalysts in the presence of trace carbon monoxide. *J. Electroanal. Chem.* 1995;391:119-123.
- [6] A. S. Arico, S. Srinivasan and V. Antonucci. DMFCs: From Fundamental Aspects to Technology Development. *Fuel Cells* 2001;1:133-161.
- [7] S. Park, A. Wieckowski and M. J. Weaver. Electrochemical Infrared Characterization of CO Domains on Ruthenium-Decorated Platinum Nanoparticles. *J. Am. Chem. Soc.* 2003;125:2282-2290.
- [8] K. Miyazaki, Y. Nishida, K. Matsuoka, Y. Iriyama, T. Abe, M. Matsuoka, K. Kikuchi and Z. Ogumi. Influence of Supporting Materials on Catalytic Activities of Gold Nanoparticles as CO-Tolerant Catalysts in DMFC. *Electrochemistry* 2007;75:217-220.
- [9] T. J. Schmidt, M. Noeske, H. A. Gasteiger, R. J. Behm, P. Brita, W. Brijoux and H. Bonnemann. Electrocatalytic Activity of PtRu Alloy Colloids for CO and CO/H<sub>2</sub> Electrooxidation: Stripping Voltammetry and Rotating Disk Measurements. *Langmuir* 1997;13:2591-2595.

- [10] Z. L. Liu, X. Y. Ling, X. D. Su and J. Y. Lee. Carbon-Supported Pt and PtRu Nanoparticles as Catalysts for a Direct Methanol Fuel Cell. *J. Phys. Chem. B* 2004;108:8234-8240.
- [11] C. Hardacre, T. Rayment and R. M. Lambert. Platinum/Ceria CO Oxidation Catalysts Derived from Pt/Ce Crystalline Alloy Precursors. *J. Catal.* 1996;158:102-108.
- [12] L. V. Mattos, E. R. de Oliveira, P. D. Resende, F. B. Noronha and F. B. Passos. Partial oxidation of methane on Pt/Ce–ZrO<sub>2</sub> catalysts. *Catal. Today* 2002;77:245-256.
- [13] M. Gotz and H. Wendt. Binary and ternary anode catalyst formulations including the elements W, Sn and Mo for PEMFCs operated on methanol or reformat gas. *Electrochim. Acta* 1998;43:3637-3644.
- [14] Y. Dai, Y. W. Liu and S. L. Chen. Pt–W bimetallic alloys as CO-tolerant PEMFC anode catalysts. *Electrochim. Acta* 2013;89:744-748.
- [15] B. N. Grgur, G. Zhuang, N. M. Markovic and P. N. Ross. Electrooxidation of H<sub>2</sub>/CO Mixtures on a Well-Characterised Pt<sub>75</sub>Mo<sub>25</sub> Alloy Surface. *J. Phys. Chem. B* 1997;101:3910-3913.
- [16] B. N. Grgur, N. M. Markovic and P. N. Ross. Electrooxidation of H<sub>2</sub>, CO, and H<sub>2</sub>/CO Mixtures on a Well-Characterized Pt<sub>70</sub>Mo<sub>30</sub> Bulk Alloy Electrode. *J. Phys. Chem. B* 1998;102:2494-2501.
- [17] Z. F. Liu, J. E. Hu, Q. Wang, K. Gaskell, A. I. Frebkel, G. S. Jackson and B. Eichhorn. PtMo Alloy and MoO<sub>x</sub>@Pt Core-Shell Nanoparticles as Highly CO-Tolerant Electrocatalysts. *J. Am. Chem. Soc.* 2009;131:6924-6925.
- [18] P. Justin and G. R. Rao. Methanol oxidation on MoO<sub>3</sub> promoted Pt/C electrocatalyst. *Int. J. Hydrogen Energy* 2011;36:5875-5884.
- [19] Z. M. Cui, S. P. Jiang and C. M. Li. Highly dispersed MoO<sub>x</sub> on carbon nanotube as support for high performance Pt catalyst towards methanol oxidation. *Chem. Commun.* 2011;47:8418-8420.
- [20] T. Ioroi, N. Fujirara, Z. Siroma, K. Yasuda and Y. Miyazaki. Platinum and molybdenum oxide deposited carbon electrocatalyst for oxidation of hydrogen

- containing carbon monoxide. *Electrochem. Commun.* 2002;4:442-446.
- [21] K. Miyazaki, K. Matsuoka, Y. Iriyama, T. Abe and Z. Ogumi. Electro-oxidation of Methanol on Gold Nanoparticles Supported on Pt/MoO<sub>x</sub>/C. *J. Electrochem. Soc.* 2005;152:A1870-A1873.
- [22] R. Vellacheri, S. M. Unni, S. Nahire, U. K. Kharul and S. Kurungot. Pt–MoO<sub>x</sub>-carbon nanotube redox couple based electrocatalyst as a potential partner with polybenzimidazole membrane for high temperature Polymer Electrolyte Membrane Fuel Cell applications. *Electrochim. Acta* 2010;55:2878-2887.
- [23] N. Tsiouvaras, M. V. Martinez-Huerta, R. Moliner, M. J. Lazaro, J. L. Rodriguez, E. Pastor, M. A. Pena and J. L. G. Fierro. CO tolerant PtRu–MoO<sub>x</sub> nanoparticles supported on carbon nanofibers for direct methanol fuel cells. *J. Power Sources* 2009;186:299-304.
- [24] T. Huang, J. H. Zhuang and Y. Yu. Electro-oxidation of methanol on co-deposited Pt–MoO<sub>x</sub> prepared by cyclic voltammetry with different scanning potential ranges. *J. Appl. Electrochem.* 2009;39:1053-1058.
- [25] L. Ma, X. Zhao, F. Z. Si, C. P. Liu, J. H. Liao, L. Liang and W. Xing. A comparative study of Pt/C and Pt–MoO<sub>x</sub>/C catalysts with various compositions for methanol electro-oxidation. *Electrochim. Acta* 2010;55:9105-9112.
- [26] M. Koyano, A. Miyata and H. Hara. Anisotropic behavior of electrical conductivity and collective motion of charge density wave in quasi-two-dimensional conductor g-Mo<sub>4</sub>O<sub>11</sub>. *Physica B: Condensed Matter* 2000;284-248:1663-1664.
- [27] T. Sato, T. Dobashi, H. Komatsu, T. Takahashi and M. Koyano. Electronic structure of η-Mo<sub>4</sub>O<sub>11</sub> studied by high-resolution angle-resolved photoemission spectroscopy. *J. Electron. Spectrosc. Relat. Phenom.* 2005;144-147:549-552.
- [28] M. S. da Luz, A. de Campos, B. D. White, J. J. Neumeier. Electrical resistivity, high-resolution thermal expansion, and heat capacity measurements of the charge-density wave compound gamma-Mo<sub>4</sub>O<sub>11</sub>. *Phys. Rev. B* 2009;79:233106-1-233106-4.

- [29] C. H. Yao, F. Li, X. Li and D. G. Xia. Fiber-like nanostructured  $\text{Ti}_4\text{O}_7$  used as durable fuel cell catalyst support in oxygen reduction catalysis. *J. Mater. Chem.* 2012;22:16560-16565.
- [30] T. Ressler, R. E. Jentoft, J. Wienold, m. m. Guinter and O. Timpe. In Situ XAS and XRD Studies on the Formation of Mo Suboxides during Reduction of  $\text{MoO}_3$ . *J. Phys. Chem. B* 2000;104:6360-6370.
- [31] T. Ressler. Reply to “Kinetics and Mechanism of  $\text{MoO}_3$  Reduction”. Comments on “In Situ XAS and XRD Studies on the Formation of Mo Suboxides during Reduction of  $\text{MoO}_3$ ”. *J. Phys. Chem. B* 2002;106:7719-7720.
- [32] Y. Wang L. J. Zhang, M. M. Zhang and F. Li. Block copolymer reduces, protects and mediates oriented growth into nano/submicron branched platinum. *J. Mater. Chem.* 2012;22:12313-12318.
- [33] Y. Wang, L. J. Zhang, F. Li, B. S. Gu. A novel Pt nanosponge foil with high activity for oxygen reduction reaction. *Electrochim. Acta* 2013;102:1-7.
- [34] H. Noh, D. Wang, S. Luo, T. B. Flanagan, R. Balasubramaniam and Y. Sakamoto. Hydrogen Bronze Formation within  $\text{Pd}/\text{MoO}_3$  Composites. *J. Phys. Chem. B* 2004;108:310-319.
- [35] P. A. Zosimova, A. V. Smirnov, S. N. Nesterenko, V. V. Yuschenko, W. Sinkler, J. Kocak, J. Holmgren and I. I. Ivanova. Synthesis, Characterization, and Sulfur Tolerance of  $\text{Pt-MoO}_x$  Catalysts Prepared from Pt-Mo Alloy Precursors. *J. Phys. Chem. C* 2007;111:14790-14798.
- [36] B. Braida, S. Adams and E. Canadell. Concerning the Structure of Hydrogen Molybdenum Bronze Phase III. A Combined Theoretical-Experimental Study. *Chem. Mater.* 2005;17:5957-5969.
- [37] L. Chen, A. C. Cooper, G. P. Pez and H. Cheng. On the Mechanisms of Hydrogen Spillover in  $\text{MoO}_3$ . *J. Phys. Chem. C* 2008;112:1755-1758.
- [38] H.B. Yu, J.H. Kim, H. Lee, M.A. Scibioh, J. Lee, J. Han, S.P. Yoon and H.Y. Ha. Development of nanophase  $\text{CeO}_2\text{-Pt}/\text{C}$  cathode catalyst for direct methanol fuel cell. *J. Power Sources* 2005;140:59-65.
- [39] N.R. Elezovic, B.M. Babic, V.R. Radmilovic, L.M. Vracar, N.V. Krstajic.

Synthesis and characterization of  $\text{MoO}_x\text{-Pt/C}$  and  $\text{TiO}_x\text{-Pt/C}$  nano-catalysts for oxygen reduction. *Electrochim. Acta* 2009;54:2404-2409.

Supporting information (SI)

### Enhanced Electrocatalytic Performance for Methanol Oxidation with a Magnéli Phase Molybdenum Oxide/Pt-black Composite

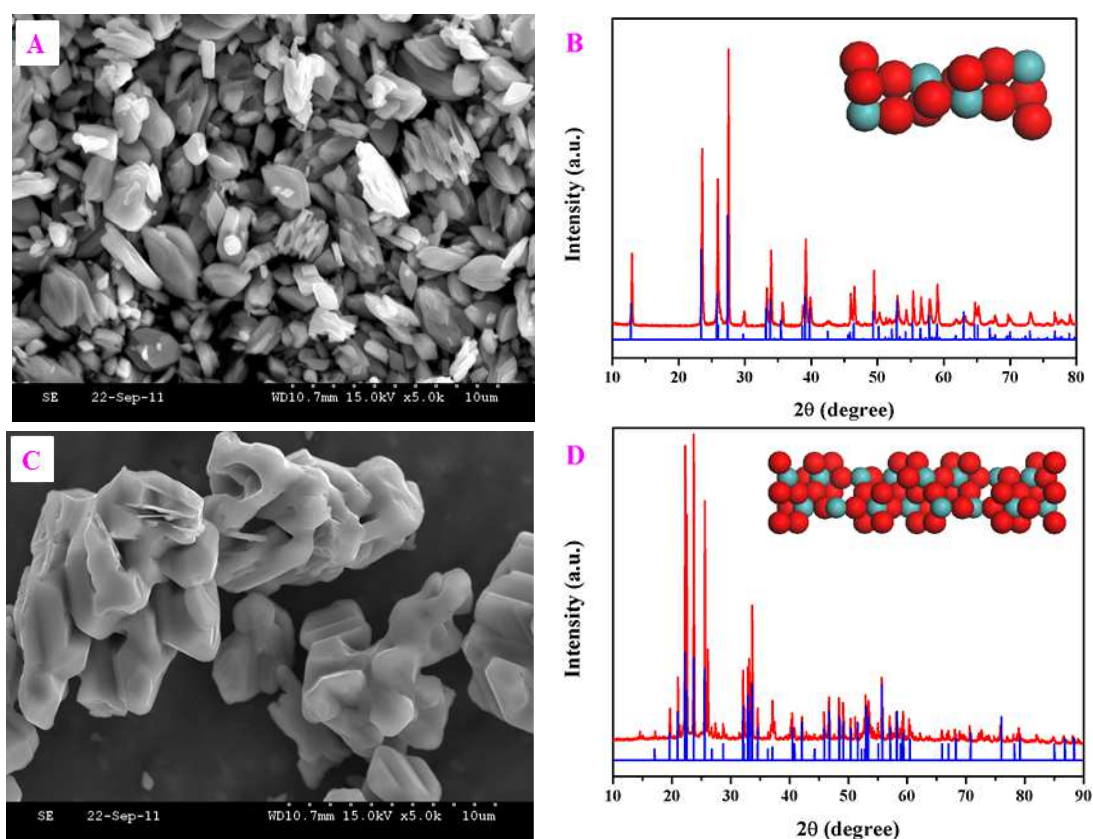


**Fig. S1** (A) Scanning electron microscope (SEM) image and (B) XRD pattern of  $\text{MoO}_3$  precursor; (C) SEM image and (D) XRD pattern of  $\text{Mo}_4\text{O}_{11}$ .

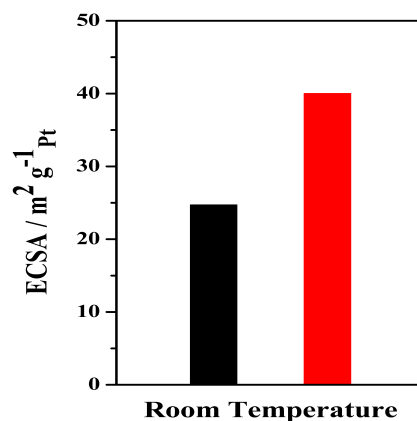


**Fig. S2** Histogram of the specific ECSA of the Pt-black (black) and Pt/ $\text{Mo}_4\text{O}_{11}$  (red).

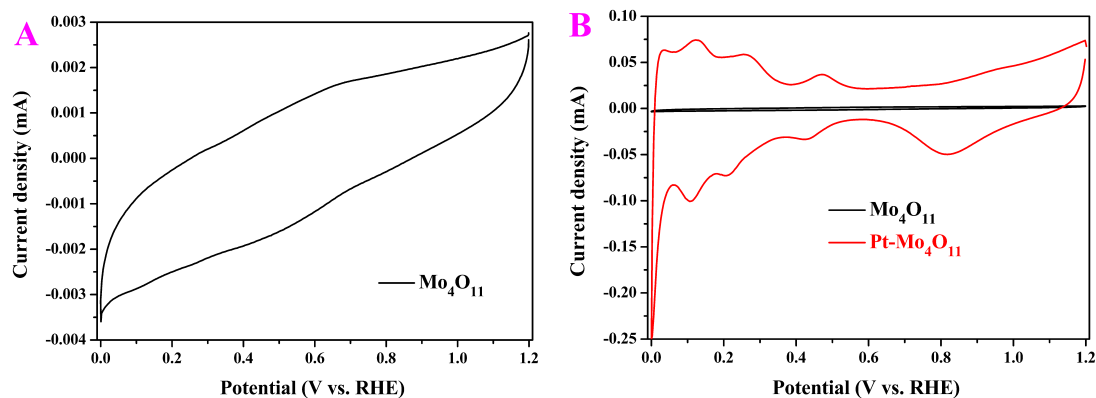


**Fig. S3** CV curves of  $\text{Mo}_4\text{O}_{11}$  and Pt/ $\text{Mo}_4\text{O}_{11}$  recorded in an Ar-purged 0.1 M  $\text{HClO}_4$  solution at a sweep rate of  $100 \text{ mV}\cdot\text{s}^{-1}$ .  $\text{Mo}_4\text{O}_{11}$  loading were 10 and  $10.4 \mu\text{g}$  for  $\text{Mo}_4\text{O}_{11}$  and Pt/  $\text{Mo}_4\text{O}_{11}$ , respectively. (A)  $\text{Mo}_4\text{O}_{11}$ , (B) Pt/ $\text{Mo}_4\text{O}_{11}$  (red) and  $\text{Mo}_4\text{O}_{11}$  (black).

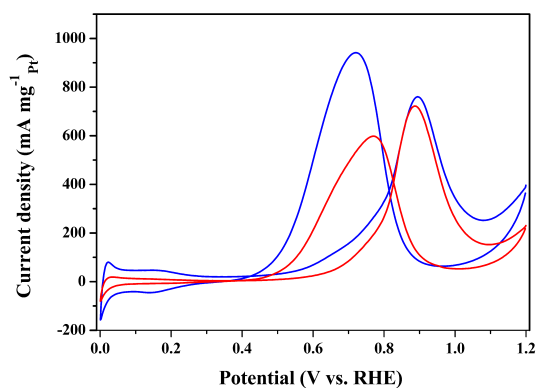


**Fig. S4** CV curves of Pt/ $\text{Mo}_4\text{O}_{11}$  (red) and Pt/C (blue) recorded in a 0.1 M  $\text{HClO}_4$  and 0.1 M  $\text{CH}_3\text{OH}$  mixed solution at a sweep rate of  $100 \text{ mV}\cdot\text{s}^{-1}$  under ambient atmosphere. Pt loading were  $2.6 \mu\text{g}$  and  $2.4 \mu\text{g}$  for Pt/ $\text{Mo}_4\text{O}_{11}$  and Pt/C, respectively.

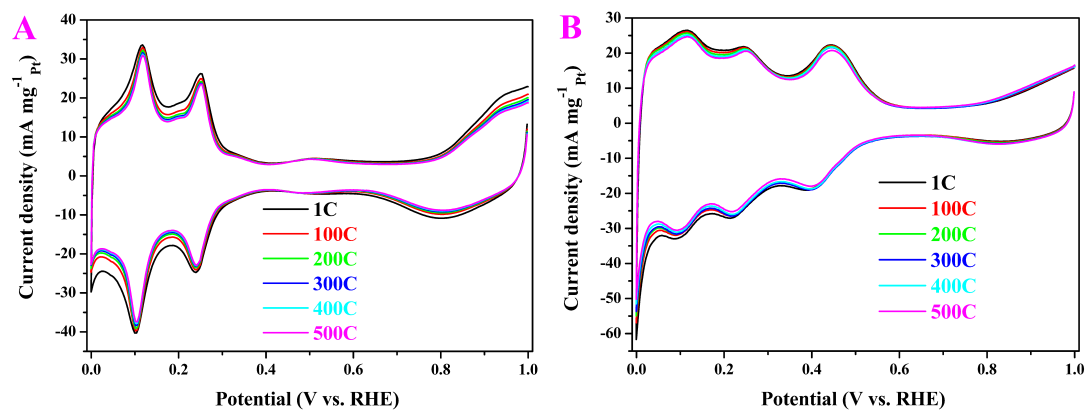


**Fig. S5** CV curves recorded in an Ar-purged  $0.1 \text{ molL}^{-1} \text{ HClO}_4$  solution with a sweep rate of  $100 \text{ mV}\cdot\text{s}^{-1}$ . Pt loading were 2 and  $13 \mu\text{g}$  for Pt/Mo<sub>4</sub>O<sub>11</sub> and Pt-black, respectively. (A) CV curves of Pt-black before and after a 500-cycle durability test, (B) CV curves of Pt/Mo<sub>4</sub>O<sub>11</sub> before and after a 500-cycle durability test.

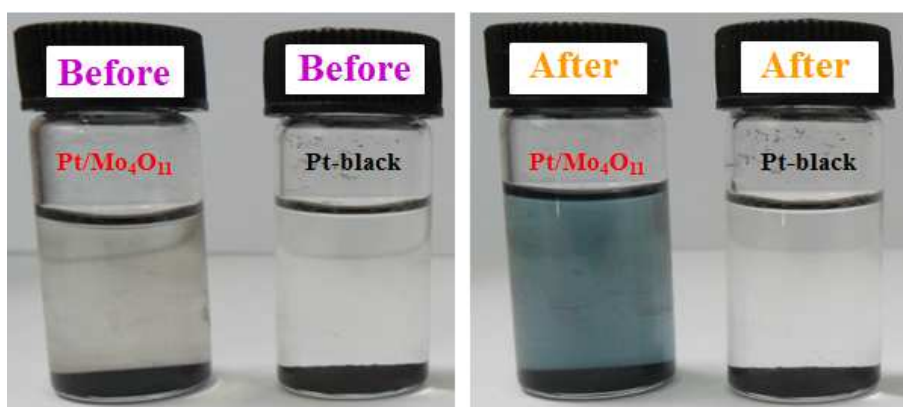


**Fig. S6** Photograph of the aqueous of Pt/Mo<sub>4</sub>O<sub>11</sub> and Pt-black in  $0.1 \text{ molL}^{-1} \text{ HClO}_4$  solution before and after standing for one week under hydrogen atmosphere.

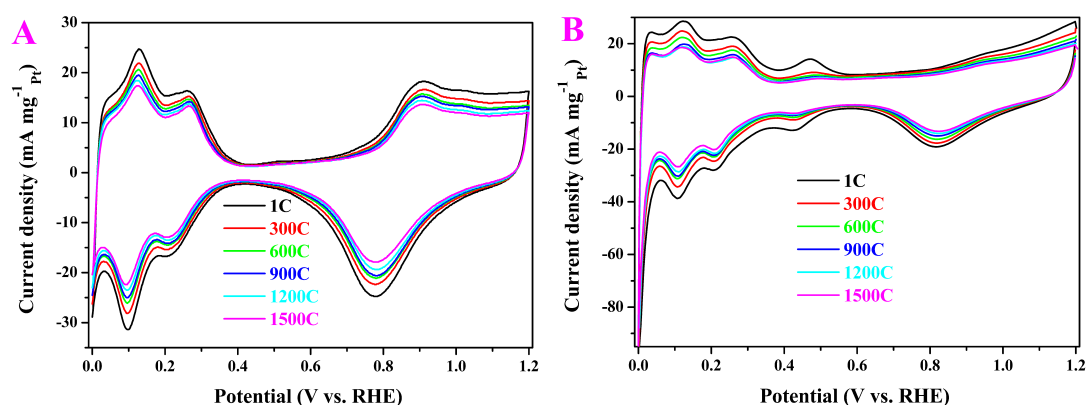


**Fig. S7** CV curves recorded in an Ar-purged  $0.1 \text{ molL}^{-1} \text{ HClO}_4$  solution with a sweep rate of  $100 \text{ mV}\cdot\text{s}^{-1}$ . Pt loading were  $8 \mu\text{g}$  and  $2.6 \mu\text{g}$  for Pt-black and Pt/Mo<sub>4</sub>O<sub>11</sub>, respectively. (A) CV curves of Pt-black before and after a 1500-cycle durability test, (B) CV curves of Pt/Mo<sub>4</sub>O<sub>11</sub> before and after a 1500-cycle durability test.

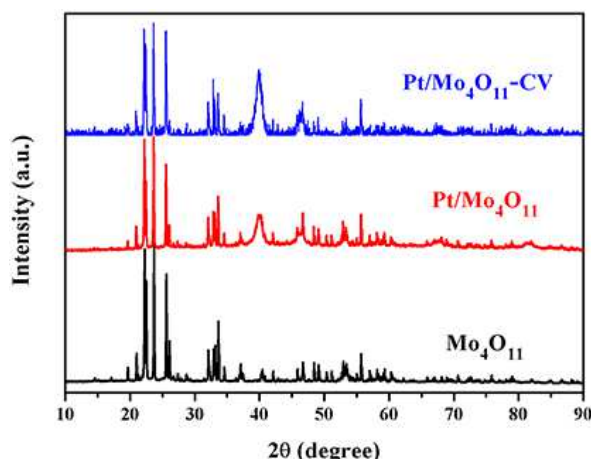


**Fig. S8** XRD patterns of Mo<sub>4</sub>O<sub>11</sub> and Pt/Mo<sub>4</sub>O<sub>11</sub> before and after a 1500-cycle durability test, respectively.

The change in the Pt-crystal size was calculated from the Pt (111) peak in XRD analysis based on Scherrer equation, as follows:

$$D = \frac{K\gamma}{B \cos \theta}$$

Where  $K$  is a dimensionless shape factor,  $K=0.89$ .  $\gamma$  is X ray wavelength,  $\gamma=0.154056$  nm.  $\beta$  is the line broadening at half the maximum intensity (FWHM).  $\theta$  is the Bragg angle.  $D$  is the mean size of the ordered (crystalline) domains, which may be smaller or equal to the grain size.

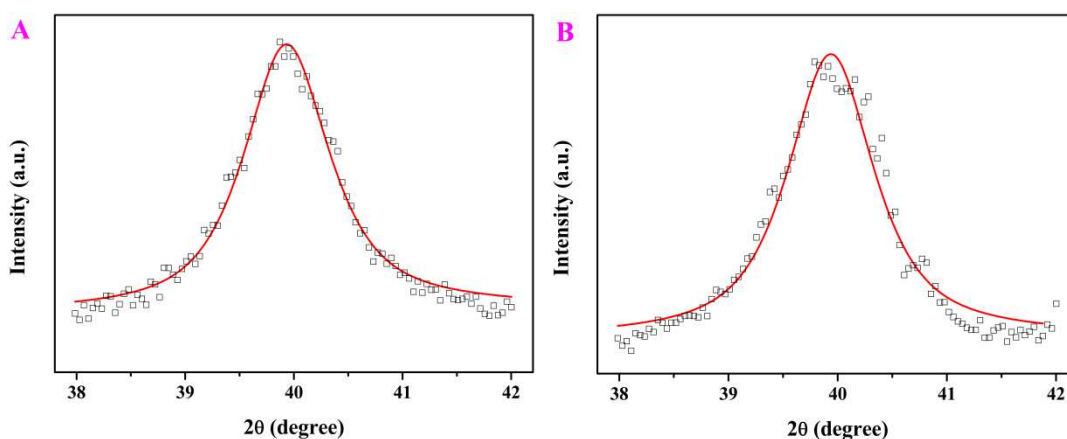


**Fig. S9** Pt (111) peak in the XRD of (A) Pt/Mo<sub>4</sub>O<sub>11</sub> and (B) Pt/Mo<sub>4</sub>O<sub>11</sub>-CV, respectively. The red line is the fitting curve.

The average crystallite sizes of Pt nanoparticles on the Mo<sub>4</sub>O<sub>11</sub> support before and after a 1500-cycle durability test are ca. 7 and 8 nm, respectively. This shows that there was a slight aggregation of Pt nanoparticles after the durability test, which

corresponds to the reduction of electrocatalyst activity.

**Table S1.** Binding energy (3d, eV) and atomic content (%) of different Mo valence states [Mo(IV), Mo(V), Mo(VI)] obtained from the Mo3d XPS spectra.

	Sample	Mo <sup>4+</sup>	Mo <sup>5+</sup>	Mo <sup>6+</sup>
<b>Mo<sub>4</sub>O<sub>11</sub></b>	Binding energy	230.11	232.66	233.11
	Content	7.09	70.74	22.17
<b>Pt/Mo<sub>4</sub>O<sub>11</sub></b>	Binding energy	231.80	232.80	233.23
	Content	3.99	80.01	16.00
<b>Pt/Mo<sub>4</sub>O<sub>11</sub>-CV</b>	Binding energy	229.93	233.00	233.39
	Content	1.47	44.94	53.59

In the mechanical mixing of Pt-black and Mo<sub>4</sub>O<sub>11</sub> support, Mo<sub>4</sub>O<sub>11</sub> would occur comproportionation ( $\text{Mo}^{+4} + \text{Mo}^{+6} \rightarrow 2\text{Mo}^{+5}$ ). The content of Mo(IV) specie in Pt/Mo<sub>4</sub>O<sub>11</sub> catalyst (3.99%) was decreased compare to Mo<sub>4</sub>O<sub>11</sub> support (7.09%). In theory, Mo<sup>+4</sup> and Mo<sup>+6</sup> should be equal to the amount of reduction in the same comproportionation. But Mo<sup>+6</sup> (6.17%) decreased much more than that of Mo<sup>+4</sup> (3.1%), which proves that a strong interaction between Pt and Mo<sub>4</sub>O<sub>11</sub>. Comparison of Fig. 3A suggested that the binding energy of Pt 4f for Pt/Mo<sub>4</sub>O<sub>11</sub> depends on the blue shifts (71.52eV). This phenomenon shows that the oxidation state of Pt increases in Pt/Mo<sub>4</sub>O<sub>11</sub> catalyst. That is to say, the electronic of Pt will delocalize to Mo<sub>4</sub>O<sub>11</sub> to reduce Mo<sup>+6</sup> ( $\text{Mo}^{+6} + \text{e}^{-1} \rightarrow \text{Mo}^{+5}$ ). This strong interaction between Pt and Mo<sub>4</sub>O<sub>11</sub> leads to the unequal reduction of Mo<sup>+4</sup> and Mo<sup>+6</sup>, naturally.

**Table S2** Comparison of the electrochemical activities of Pt/Mo<sub>4</sub>O<sub>11</sub>, Pt-black and Pt/C.

sample	I <sub>f</sub> potential (V)	I <sub>f</sub> current (mA·mg <sup>-1</sup> <sub>Pt</sub> )	I <sub>b</sub> potential (V)	I <sub>b</sub> current (mA·mg <sup>-1</sup> <sub>Pt</sub> )	I <sub>f</sub> /I <sub>b</sub>
<b>Pt-black</b>	0.93	356.10	0.81	380.43	0.94
<b>Pt/C</b>	0.90	823.65	0.72	1019.81	0.81

---

<b>Pt/ Mo<sub>4</sub>O<sub>11</sub></b>	0.87	722.20	0.77	598.29	1.21
---	------	--------	------	--------	------

---

HIDDEN TEXT FOUND PLEASE VERIFY IT FROM INPUT DOC FILE THEN DELETE IT IF NOT

REQUIRE:.....\*\*\*\*\*